Alteration of nociceptive Schwann cells in a mouse model of high-fat diet induced diabetic peripheral neuropathy

Guillaume Rastoldo[1], Ali K. Jaafar[1], Aurélie-Paulo-Ramos[1], Katy Thouvenot[1], Cynthia Planesse[1], Matthieu Bringart[1], Marie-Paule Gonthier, Gilles Lambert and Steeve Bourane[1]*

1- Université de La Réunion, INSERM, UMR 1188 Diabète athérothrombose Réunion Océan Indien (DéTROI), Saint-Pierre, La Réunion, France.

Abstract

Diabetic peripheral neuropathy (DPN) is characterized by progressive and symmetrical sensory abnormalities and constitutes one of the earliest and main complications of diabetes. DPN is characterized by heterogeneous sensory symptoms such as chronic pain, tingling, burning or loss of sensation. Nociceptive Schwann cells (nSCs), a recently identified subtypes of dermal Schwann cells support terminal nerve fibers in mouse skin and contribute to mechanical sensation and neuropathic pain. While terminal nerve fibers density is evaluated in DPN models, there is currently no data about nSCs number and integrity during the early stages of the disease. In the present study, we determined the quantitative differences in terminal nerve fiber density as well as nSCs number and cellular extensions between control and high-fat diet (HFD) induced diabetic mice presenting with a neuropathic phenotype. We also characterized L1CAM as a reliable and specific marker of nSCs, a cell type previously assessed by the expression of S100β and Sox10. Interestingly, we observed a decrease in intraepidermal nerve fiber density (IENFD) associated with a significant reduction of nSCs in the glabrous foot skin of neuropathic mice. Overall, this study identifies L1CAM as a new marker of nSCs and indicates that these cells are impacted in diabetic peripheral neuropathy.

Keywords: DPN; Nociceptive Schwann Cells; Type 2 diabetes; Mechanical hypoalgesia; Thermal hyperalgesia

Word count: 3431

Introduction

One of the first and main complications of diabetes is diabetic peripheral neuropathy (DPN), affecting more than 60% of diabetic patients [1]. DPN involves damage to the peripheral nervous system, i.e., the sensory and motor nerves as well as the autonomic nervous system that control our organs. The most common symptoms of DPN are an impairment of sensitivity to pain and touch [2]. The early stages of the pathology are characterized by abnormal sensory symptoms such as pain, tingling, burning sensations, electrical discharges, pain evoked by non-painful mechanical stimuli (allodynia), increased sensitivity to noxious stimuli (hyperalgesia) [2] significantly altering the patients' quality of life. Other sensory deficits such as numbness are also observed with progressive loss of sensation in the lower limbs often leading to tissue damage with the development of ulcers, increasing the risk of amputation [3][4]. Reduced sensations in the foot also lead to progressive loss of balance resulting in an increased risk of falls [5, 6].

Despite decades of research, there is currently no effective treatment for DPN due to an incomplete understanding of the underlying molecular and cellular mechanisms. Much attention has been dedicated to the damage of small, non-myelinated nerve fibers (C-fibers) responsible for sensitivity to heat and pain. The degeneration and regeneration of these fibers are typical features of diabetes skin biopsy analyses serve as late-stage confirmations of DPN presence [7]. While C-fibers were traditionally believed to terminate freely in the epidermis, recent work by Abdo et al. challenged this concept [8]. Their findings reveal a close connection between C-fibers and specialized nociceptive Schwann cells (nSC) capable of independently generating pain signals. These cells are currently identified by the expression of S100β and Sox10 [9–11] and most importantly, eliminating nSC alone is sufficient to induce neuropathic pain in mice [11]. Considering these recent breakthroughs, we hypothesize that neuropathies involving C-fiber degeneration, as seen in DPN, may result from damages to nSCs, as suggested by a recent report demonstrating a decrease in nSC density in Streptozotocin-induced type 1 diabetic mice [9]. To date, no study has evaluated the integrity of nSC in a type 2 diabetes model. We have therefore explored the impact of type 2 diabetes on the integrity of nSC during DPN pathology development.

Methods

Research Design

All reported experiments were performed at the GIP-CYROI platform's animal facility, conducted in accordance with the French and European Community Guidelines for the Use of Animals in Research (86/609/EEC and 2010/63/EU), and were approved by the local Ethics

Committee (n°114) for animal experimentation and the French authorities (APAFIS#31763-2018020912188806, approved on May 21, 2021).

Animals

Twenty C57BL/6J mice (male, 6 weeks old) were purchased from Janvier (Le Genest Saint Isle, France) and housed (5 mice per cage) in a temperature-controlled environment with a 12–12h light/dark photocycle. After 2 weeks of adaptation, mice were divided in two groups (n=10/group) and placed either on a control diet (10% kcal %fat; SF13-081) or a high-fat diet (45% kcal %fat; SF04-001) from Specialty Feeds during 16 weeks. Mice with fasting blood glucose above ≥ 200 mg/dL were considered diabetic [12].

Mice expressing a tamoxifen-inducible Cre recombinase under the control of the PLP promoter (PLP-CreER^{T2}; [13]) were crossed to Ai14 mice, which have a LoxP-flanked stop cassette excisable by Cre. At 6 weeks of age, the PLP-CreER^{T2}; Ai14 progeny were injected intraperitoneally with tamoxifen (100 µg/g of mice) for 5 consecutive days. Tamoxifen was prepared in a mixture of 9/10 corn oil and 1/10 ethanol, and stored at 4 °C in a light-proof container. After 2 weeks, the mice were euthanized and the tissue collected for immunostaining.

Genotyping

Genotyping of progeny from PLP-CreER^{T2} and Ai14 mice were done with PCR using CreDN2 (GAT CTC CGG TAT TGA AAC TCC AGC), CreUP2 (GCT AAA CAT GCT TCA TCG TCG G), Ai14mut-Fwd (CTG TTC CTG TAC GGC ATG G) and Ai14mut-Rev (GGC ATT AAA GCA GCG TAT CC) primers.

Oral glucose tolerance test (OGTT)

An OGTT was performed after 16 weeks of diet in all mice. After 6 hours of fasting, one drop of tail blood was collected and glycemia was analyzed using a standard glucometer (One Touch Profile, Lifescan Inc., Milpitas, CA, USA, #6 strips). Oral gavage with glucose 30% (2g/kg body weight) into conscious mice was performed and glycemic levels measured 15, 30, 45, 60, 90 and 120 min post-administration.

Nerve conduction velocity

Mice were anesthetized by using isoflurane (IsoFlo®, Centravet, France) and placed on a heating pad. Once anesthetized, motor nerve conduction velocities (MNCV) and sensory nerve conduction velocities (SNCV) were determined as previously described [14–16]. Using the Keypoint 4, Dantec-Medtronic electroneuromyography device, we performed both proximal

102 and distal nerve stimulations of the sciatic nerve, registering the transmitted potentials with
103 sensing electrodes at the gastrocnemius muscle. We used stainless steel subdermal needle
104 electrodes to deliver single square-wave supramaximal stimulation with 0.2 millisecond
105 impulses. MNCV was calculated by subtracting the distal from the proximal latency (measured
106 in milliseconds) from the stimulus artifact of the take-off of the evoked potential, and the
107 difference was divided into the distance between both stimulating electrodes (measured in
108 millimeters using a Vernier caliper). For SNCV, recording electrodes were placed on the
109 dorsum of the foot and stimulating electrodes on the ankle. The latency of onset (milliseconds)
110 of the sensory nerve action potential after supramaximal antidromic stimulation of the sural
111 nerve at the ankle was divided by the distance between the recording and stimulation
112 electrodes (measured in millimeters using a Vernier caliper).
113

114 **Tissue Harvest**

115 After 16 weeks of diet, mice received a subcutaneous injection of Buprenorphine (0.05 mg/kg,
116 Buprecare®, Centravet, France) and were anesthetized by using isoflurane (3%). Mice were
117 then euthanized by intracardiac puncture and blood samples were collected and centrifuged
118 at 2000 rpm for 10 min at 4°C. Serum was collected and stored at −80°C until analysis.
119 Intracardiac perfusion was performed with 20 mL of phosphate buffered saline (PBS) and 20
120 mL of 4% paraformaldehyde (PFA) dissolved in PBS. The hind-paw plantar surfaces of each
121 mouse were collected and post-fixed overnight in 4% PFA solution. Biopsies of foot skin were
122 then rinsed and cryoprotected into 30% sucrose dissolved in PBS at 4°C. The samples were
123 then embedded in optimal cutting temperature (OCT, Tissue-Tek®, USA) compound and
124 stored at −80°C until sectioning.

125

126 **Immunohistochemistry**

127 Tissus sections (30 µm) were collected from the hind-paw plantar surface and washed
128 (3x10min) with PBS. Blocking and permeabilization were done by incubation (1h) in 5% donkey
129 anti-serum and 0.3% Triton X-100. For intraepidermal nerve fibers density, sections were
130 incubated with the primary antibody anti-PGP9.5 (1:500, #14730-1-AP, ProteinTech) for 2
131 days; first overnight at 4°C and the next day sections were incubated overnight at room
132 temperature. The same protocol was applied for L1 cell adhesion molecule (L1CAM, 1:500,
133 #20659-1-AP, ProteinTech) antibody but the sections were incubated only overnight at 4°C.
134 Sections were then rinsed in PBT (PBS + 0.1% triton) and incubated for 1 h at room
135 temperature with the secondary antibody Alexa Fluor 594 donkey anti-rabbit (1:500, Abcam;
136 ab150064), or Alexa Fluor 488 donkey anti-Rabbit (1:500, Invitrogen; A-21206).

137

138 **Identification and quantification of nociceptive Schwann cells**

Nociceptive Schwann cells were identified according to Hu et al. criteria [9]. Commonly, nSCs connect to PGP9.5+ nerve endings and are located within 25 µm depth in the subepidermal zone at the junction between dermis and epidermis. For quantification, we excluded L1CAM positive staining in glands or large peripheral fiber bundles found deeper in the dermis. The number of nSCs was reported per mm length of foot skin. To quantify nSCs cellular extensions, we measured cell fluorescence using ImageJ. We selected the region of interest (ROI) at the subepidermal zone in each image of the foot skin and measured the mean fluorescence value in that area using 'Mean gray value'.

Confocal imaging

Intraepidermal nerve fibers density and nociceptive Schwann cells number were evaluated under a laser scanning confocal microscope Eclipse (Nikon) with a 40x objective. Following immunostaining, 30 µm thick Z-stack images were taken and analysis was performed on orthogonal maximum intensity projection of the original confocal Z-stack images.

Metabolic markers

Plasma hemoglobin A_1C levels were determined using DCA® Vantage Analyzer (Siemens Healthineers, France) and hemoglobin A_1C reagent kit (#23-312018). Serum triglycerides (TG) and total cholesterol levels were determined using colorimetric assays (Diasys®, #157109910021 and #113009910021, Germany). Plasma insulin and leptin concentrations were measured using a mouse insulin and leptin ELISA kit (Mercodia®, #10-1247-01, Sweden and RayBiotech®, Peachtree Corners, GA, USA). All metabolic markers were measured after 16 weeks of diet.

Behavioral tests

Von Frey test

Mice were familiarized with the testing apparatus 1h/day during a week before behavioral testing. Animals were placed on an elevated wire grid and the plantar surface of the hindpaw was stimulated with calibrated von Frey monofilaments (0.008-6 g). The paw withdrawal threshold for the von Frey assay was determined by SUDO up-down method [17]. Testing was performed every 4 weeks after the start of the diet and up to 16 weeks.

Hargreaves test

To measure radiant heat pain by Hargreaves test [18], animals were put in plastic boxes and the plantar paw surface was exposed to a beam of radiant heat according to the Hargreaves

174 method. Paw withdrawal latency was then recorded and beam intensity was adjusted to result
175 in a latency around 10 seconds in control animals. Testing began after exploration and after
176 grooming behaviors ended. High speed of skin heating (6.5°C/sec) preferentially activates Aδ-
177 fibers [19]. Based on previous study [20], we used a medium to high speed of temperature
178 heating (5°C/sec during 10 sec to obtain 50°C) to predominantly activate Aδ-fibers. Testing
179 began after exploration and grooming behaviors ended. Heat stimulation was repeated 5
180 times with an interval of 10 min for each animal and the mean was calculated. A cutoff time
181 of 30 seconds was set to prevent tissue damage. Testing was performed every 4 weeks after
182 the start of the diet and up to 16 weeks.

183 *Brush Test*

184 To measure dynamic allodynia, mice were familiarized with the testing apparatus (the same
185 that for von-Frey test) 1h/day during a week before testing. A soft paintbrush (Lefranc &
186 Bourgeois® - Brush no. 4 #175160) was used to gently stroke the plantar surface of the
187 hindpaw in the direction from heel to toe. The test was repeated five times, with intervals of
188 5 min. For each test, no evoked movement was scored as 0, and walking away or occasionally
189 brief paw lifting (~1 sec or less) was scored as 1. For each mouse, the cumulative scores of the
190 five tests were used to form a percentage response (100% response equivalent to 5 evoked
191 movements during the 5 stimulations of the paw). Testing was performed every 4 weeks after
192 the start of the diet for up to 16 weeks.

193 *Pinprick Test*

194 To measure acute mechanical pain, mice were familiarized with the testing apparatus (the
195 same that for von-Frey test) 1h/day during a week before testing. After this acclimation, for
196 pinprick test, we touched the plantar surface of the hindpaw with a pin [21] and measured
197 numbers of withdrawal response as for the brush tests. For each mouse, the cumulative scores
198 of the five tests were used to form a percentage response (100% response equivalent to 5
199 evoked movements during the 5 stimulations of the paw). Testing was performed every 4
200 weeks after the start of the diet and up to 16 weeks.

201

202 **Statistical analysis**

203 We first analyzed the normality of data and showed that the results of serum triglycerides and
204 total cholesterol levels, insulinemia, motor NCV, sensory NCV, IENFD and L1CAM-positive cells
205 were normally distributed. Thus, unpaired Student's *t*-tests (two tailed) were used for
206 statistical comparisons. For behavioral data, a two-way ANOVA for repeated measures
207 followed by Bonferroni's post-hoc test was used to determine statistically significant
208 differences. A *P* value of less 0.05 was considered significant.

209

210

211 ## Results

212 *1. Body weight gain, serum triglycerides and total cholesterol levels*

213 To determine the effect of high-fat diet (HFD) on the development of peripheral neuropathy,
214 we fed mice with a control diet (10% kcal %fat) or a HFD (45% kcal %fat) for 16 weeks
215 (n=10/group, **Figure 1A**). As anticipated, HFD-fed mice gained significant more weight
216 compared with controls. The difference became significant from week 11 onward (**Figure 1B**).
217 In line with weight gain, blood samples analyses revealed that HFD-fed mice exhibited higher
218 circulating levels of leptin compared with controls (**Figure 1C**). Triglycerides levels were not
219 significantly increased (**Figure 1D**). However, HFD-fed mice showed significantly higher total
220 plasma cholesterol level than mice fed with the control diet ($P < 0.01$; **Figure 1E**).

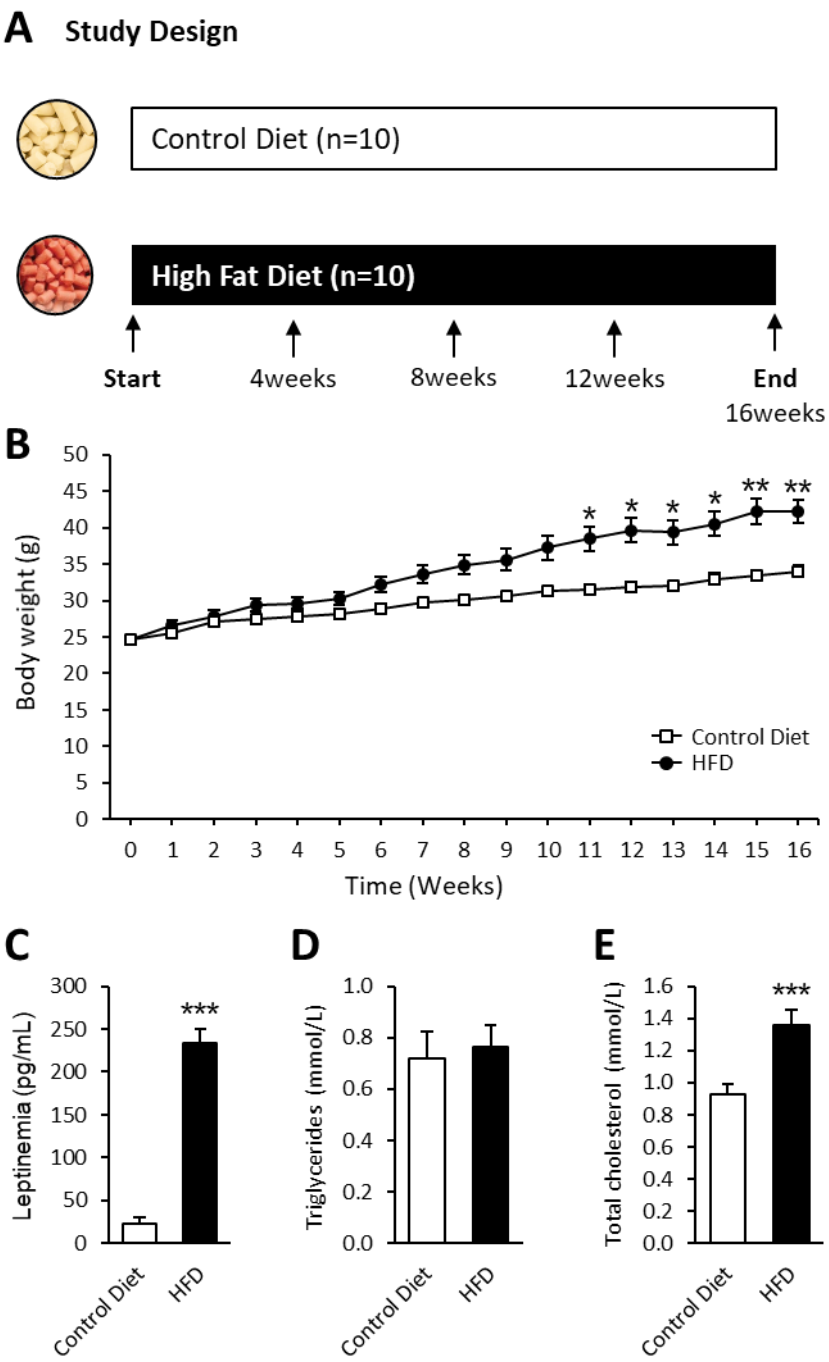

Figure 1: Study design and HFD-induced dyslipidemia. (**A**) Study Design used to assess the effect of a HFD (45% kcal %fat) vs. a control diet (10% kcal %fat) in two groups of mice (n=10/group). (**B**) Body weight of control diet-fed mice and HFD-fed mice during the 16 weeks of diet. (**C**) Leptinemia of control and HFD mice at 16 weeks of diet. (**D**) Plasma levels triglycerides of control and HFD mice at 16 weeks of diet. (**E**) Total cholesterolemia of control and HFD mice at 16 weeks of diet. *P < 0.05, **P < 0.01, ***P < 0.001: control diet vs. HFD. Data are presented as means ± SEM.

2. Glucose homeostasis / Glucose regulation

Fasting glucose levels exhibited a significant increase in HFD-fed mice compared with controls (P < 0.001; **Figure 2A**) whereas HbA1c levels were not significantly altered (**Figure 2B**). In contrast, plasma insulin levels in HFD-fed mice were significantly increased compared with controls (P < 0.001; **Figure 2C**) indicating impaired glucose tolerance and insulin resistance. We performed an oral glucose tolerance test (OGTT) after 16 weeks of diet on both groups and observed that glucose tolerance was impaired (**Figure 2D**) with the AUC of blood glucose concentrations significantly higher in HFD-fed mice compared to control diet-fed mice (P < 0.01; **Figure 2E**).

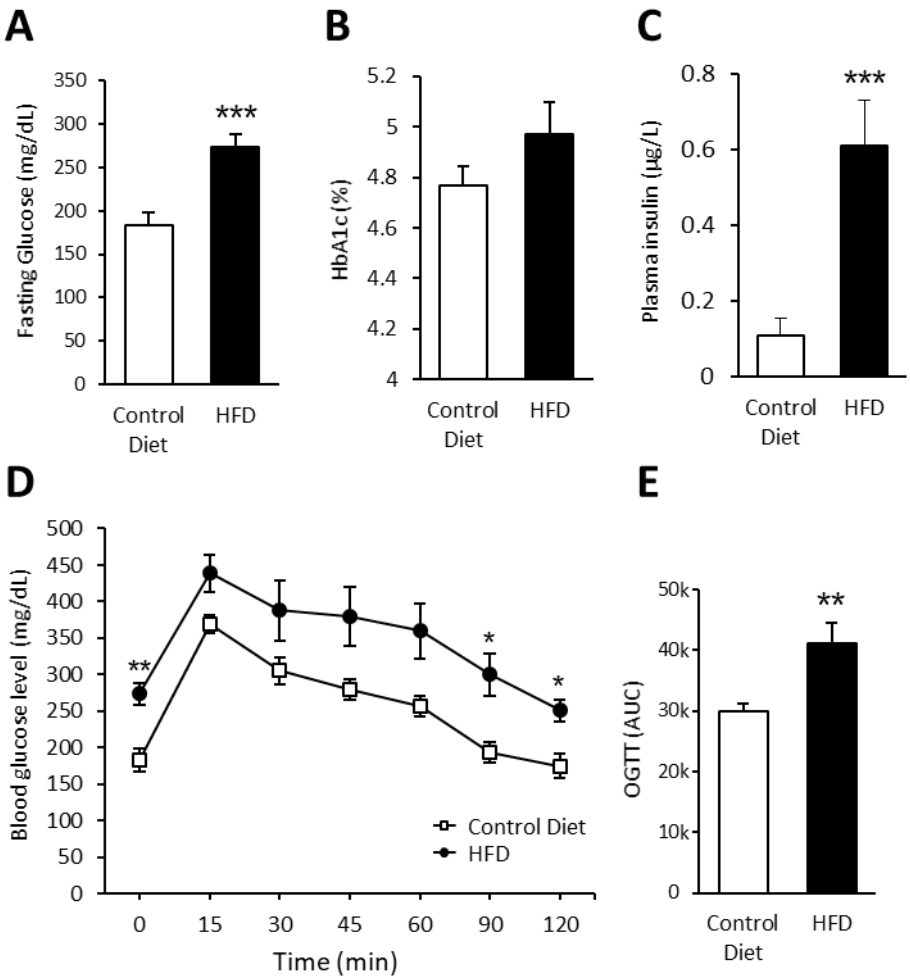

Figure 2: HFD-induced impaired glucose tolerance. (A) Fasting blood glucose of control diet-fed mice and HFD-fed mice at 16weeks of diet. **(B)** Percentage of glycated hemoglobin (HbA1c) of control diet-fed mice and HFD-fed mice at 16 weeks of diet. **(C)** Plasma insulin of control diet-fed mice and HFD-fed mice at 16 weeks of diet. **(D)** Oral glucose tolerance test (OGTT) curves performed at 16 weeks of diet in control and HFD-fed mice. **(E)** Area under the curve (AUC) during OGTT for control diet-fed mice and HFD-fed mice. *P < 0.05, **P < 0.01, ***P < 0.001: control diet vs. HFD. Data are presented as means ± SEM (n=10/group).

249

250 *3. Nerve conduction studies*

251 At week 16, nerve conduction velocity (NCV) was measured in the sciatic and sural nerves of
252 each animal. HFD-fed mice did not show any significant change in motor (**Figure 3A**) or sensory
253 (**Figure 3B**) NCV compared with controls.

254

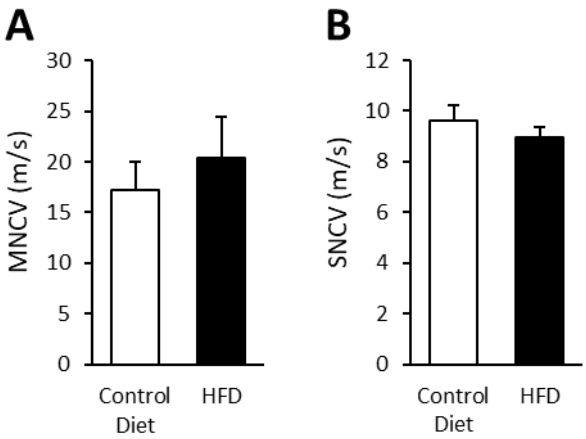

255

256 **Figure 3: Nerve conduction studies. (A)** Motor nerve conduction velocity (MNCV) performed
257 at 16 weeks of diet in control and HFD-fed mice. **(B)** Sensory nerve conduction velocity (SNCV)
258 performed at 16 weeks of diet in control and HFD-fed mice**.** Data are presented as means ±
259 SEM (n=10/group).

260

261 *4. Thermal and mechanical pain sensitivity*

262 To evaluate peripheral neuropathy we performed various behavioral sensory tests every 4
263 weeks for 16 weeks. HFD-fed mice exhibited an increase in paw withdrawal threshold as early
264 as 8 weeks (4 weeks HFD vs. 8 weeks HFD, $P < 0.01$, **Figure 4A**) and were significantly different
265 from their control diet-fed counterparts after 12 weeks of diet (12 weeks control diet vs. 12
266 weeks HFD, $P < 0.01$, **Figure 4A**), indicating a decrease in mechanical sensitivity. In parallel,
267 we observed an increase in thermal sensitivity of HFD-fed mice compared with control mice
268 from week 8 (**Figure 4B**). The latency of hind-paw withdrawal in response to noxious thermal
269 stimulus was significantly decreased in HFD-fed mice compared with control diet-fed mice at
270 12 and 16 weeks ($P < 0.001$). No significant change in haptic mechanical sensitivity (**Figure 4C**)
271 evaluated with the brush test or acute mechanical pain sensitivity (**Figure 4D**) assessed by the
272 pinprick test was noticed over 16 weeks between both groups.

273

274

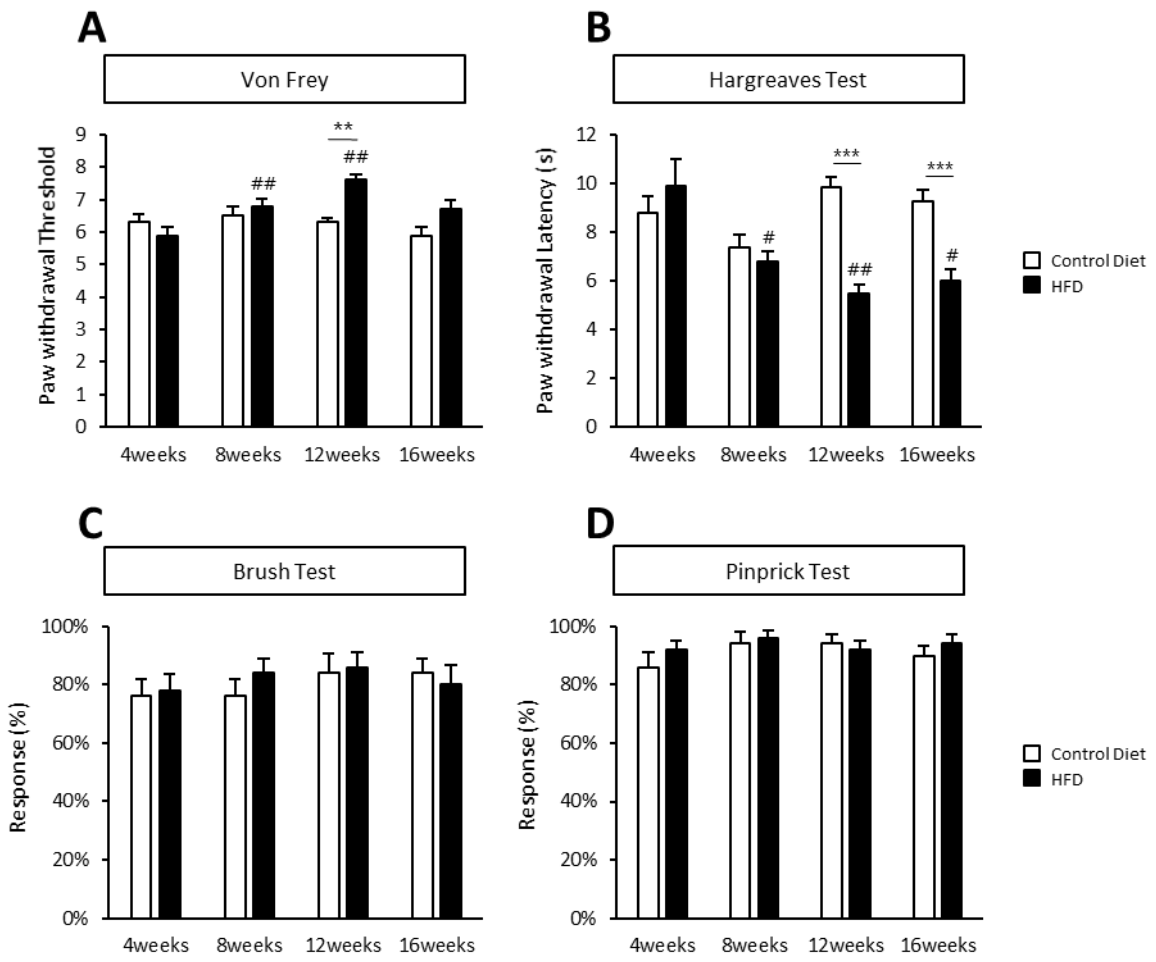

Figure 4: Mechanical and thermal sensitivity changes induced by HFD. (A) Quantification of static mechanical sensitivity was assessed every 4 weeks in control and HFD-fed mice using von Frey filaments. **(B)** Quantification of thermal sensitivity by Hargreaves test every 4 weeks in control and HFD-fed mice. **(C)** Quantification of haptic mechanical sensitivity by brush test every 4 weeks in control and HFD-fed mice. **(D)** Quantification of acute mechanical pain by pinprick test every 4 weeks in control- and HFD-fed mice. $^{**}P < 0.01$, $^{***}P < 0.001$: control diet vs. HFD. $\#P < 0.05$, $\#\#P < 0.01$: HFD 4weeks vs. HFD 8, 12 or 16 weeks. Data are presented as means ±SEM (n=10/group).

5. Epidermal innervation and Nociceptive Schwann cells

To fully characterize the neuropathic phenotype in our model, we analyzed the intraepidermal nerve fiber density (IENFD) in the glabrous skin of control and HFD-fed mice. We found a significant reduction of foot skin innervation in HFD-fed compared with control mice after 16 weeks of diet ($P < 0.001$; **Figure 5A**, **5B**). Additionally, we investigated the integrity of nociceptive Schwann cells that are present in the skin at the junction between the epidermis and the dermis by using immunohistochemistry against L1CAM that we found highly expressed in this cell type. To validate the specificity of L1CAM expression in nociceptive

293 Schwann cells, we first verified its colocalization with Sox10 and S100β, two known markers
294 of these cells [9–11] (**Figure 5C**). To further these observations, we confirmed the specific
295 expression of L1CAM in td-Tomato positive nSCs in PLP-CreER^{T2};Ai14 double transgenic mouse
296 foot skin (**Figure 5D**), [13, 22]. Altogether, these results indicate that L1CAM is a reliable and
297 specific marker of nSCs.

298 Using this new marker to identify nSCs, we observed that, both mean fluorescence intensity
299 (**Figure 5E**,**F**) and mean number of L1CAM-positive cells and cellular extensions (**Figure 5E**,**G**)
300 were significantly decreased in HFD-fed mice compared with control mice ($P < 0.001$ and $P <$
301 0.01 respectively). Altogether, these results indicate a decrease in both sensory nerve endings
302 and number of nociceptive Schwann cells in the foot skin of HFD mice.

303

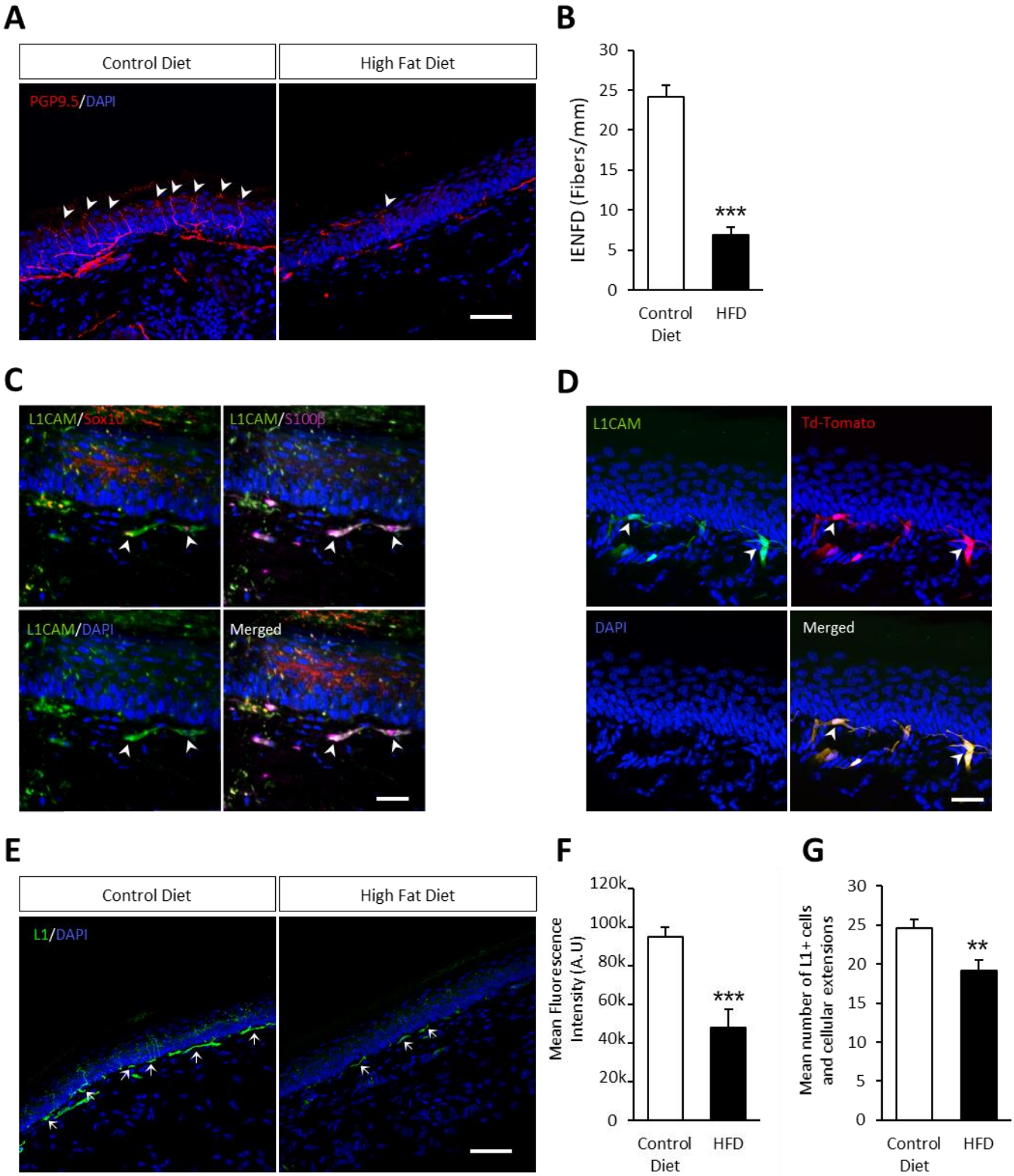

Figure 5: HFD-induced small nerve fiber and nociceptive Schwann cells degeneration in the foot skin. (A) PGP9.5 immunofluorescence with DAPI staining in foot skin section of control (n=5) and HFD-fed mice (n=5). Arrowhead indicate nerve fibers in the epidermis of the foot skin. **(B)** Quantification of IENFD is presented as the number of fibers/mm of epidermis. **(C)** L1CAM immunofluorescence colocalized with Sox10 andS100β classical markers of

310 nociceptive Schwann cells in the foot skin. **(D)** L1CAM immunofluorescence colocalized with
311 Td-tomato expressing nociceptive Schwann cells in a tamoxifen-induced PLP-
312 *Cre*ER^{T2};R26TdTomato double transgenic mouse. Arrowhead indicate nociceptive Schwann
313 cells and their cellular extensions at the border of the epidermis and dermis. **(E)** L1CAM
314 immunofluorescence with DAPI staining in foot skin section of control (n=5) and HFD-fed mice
315 (n=5). Arrows indicate nociceptive Schwann cells and their cellular extensions at the border of
316 the epidermis and the dermis. **(F)** Mean fluorescence intensity quantification of L1CAM
317 immunostaining at the localization of nociceptive Schwann cells (at the border of epidermis
318 and dermis).**(G)** Quantification of L1CAM-positive cells and their cellular extensions presented
319 in number/mm of epidermis**.** $^{**}P < 0.01$, $^{***}P < 0.001$: control diet vs. HFD. Data are
320 presented as means ± SEM. Scale bar: 50 µm.

321

322 ## Discussion

323

324 In the present study, we used HFD fed mice during 16 weeks to generate a mouse
325 model of diabetic peripheral neuropathy and compared dyslipidemia, glucose tolerance, and
326 sensory deficits of these mice with those on placed on a control diet. We observed that HFD-
327 fed mice display increased weight gain, elevated leptinemia, hypercholesterolemia, impaired
328 glucose tolerance, elevated fasting blood glucose and insulin resistance compared with
329 control-fed animals, recapitulating the metabolic dysfunctions observed in type 2 diabetes.
330 The analysis of IENFD of the foot skin revealed an important reduction in terminal nerve fibers
331 and nSCs in HFD-fed mice compared with mice fed with a control-diet, paralleling behavioral
332 sensory deficits in HFD-fed mice, with the development of mechanical hyposensitivity and
333 thermal hypersensitivity, clearly indicative of a peripheral neuropathy phenotype.

334 To characterize the progression of peripheral neuropathy, we followed the guidelines of the
335 diabetic neuropathy study group of the European Association for the Study of Diabetes.
336 Namely, we assessed three key features present in human pathology (nocifensive behavior,
337 nerve conduction velocity, and IENFD) considering that the presence of alterations in two of
338 these three parameters is necessary to establish a neuropathic phenotype in rodents [23]. In
339 this study, we demonstrate that HFD-fed mice exhibite mechanical hypoalgesia and thermal
340 hyperalgesia coupled to a severe loss of intraepidermal nerve fibers but no impairment of
341 motor or sensory nerve conduction velocity. According to the above-mentioned criteria of
342 Neurodiab, we can assert that our HFD-fed mice developed diabetic peripheral neuropathy.

343 To identify possible damages to small sensory fibers, we next performed a quantification of
344 intraepidermal nerve fibers density considered as the gold standard for the evaluation of small
345 fiber neuropathies [24]. Damage to small sensory fibers is one of the earliest manifestations
346 of DPN that can be observed in prediabetic conditions [25]. We found a 70% reduction in
347 epidermal innervation in the hind paw of the HFD-fed mice in comparison with control-fed

348 mice, in agreement with previous reports [26–28]. Studies have shown that small nerve fibers
349 penetrating the epidermis are mostly nociceptive [7] and that these fibers undergo
350 degeneration and regeneration at the early stages of type 2 diabetes in humans [5, 29]. Until
351 recently, it was thought that because unmyelinated C-fibers lack the protection and nutrient
352 supply that myelinated Schwann cells provide to A-fibers, C-fibers were more likely affected
353 at the early stages of diabetic neuropathy. However, recently a specialized cutaneous type of
354 Schwann cells, termed nociceptive Schwann cells , in close relationship with nociceptive C-
355 fibers in the dermis has been discovered [8]. These cells contribute to terminal axon support
356 and play a critical roles in skin mechano-sensitivity and neuropathic pain [10, 11, 34, 35].
357 Therefore, nociceptive endings in the epidermis are not free but form a mesh-like organ with
358 a mutual dependence between C-fibers and nSCs. The absence of nSCs induces a retraction of
359 epidermal nerve fibers and development of mechanical, cold, and heat hyperalgesia [11]. In
360 the present study, we identified L1CAM as a reliable marker for nSCs, as an alternative to the
361 conventional S100β / Sox10 staining methods [9–11]. As outlined by Hu et al., the precise
362 localization of Schwann cells serves as a crucial criteria in distinguishing nSCs [9]. These
363 distinctive cells are arranged within a 25 µm depth in the subepidermal region, excluding
364 glands and large fiber bundles. Based on these criteria and the expression of L1CAM, we
365 demonstrate a significant decrease in the number of nSCs and their cellular extensions in T2D
366 mice, as previously observed in type 1 diabetic mice [9].

367 Hyperglycemia represents a key factor that can induce apoptosis in Schwann cells [37].
368 Inhibiting apoptosis of Schwann cells under high-glucose conditions is considered a promising
369 approach to treat DPN [38]. However, glycemic control has little impact of the development
370 and progression of neuropathy in type 2 diabetic patients [39]. Dyslipidemia is another
371 frequent perturbation of T2D, but the impact of this lipids on Schwann cells integrity has
372 received relatively little attention [40–42]. The elucidation of mechanisms implicated in the
373 alteration of nSCs in HFD-fed mice therefore seems central for the future development of
374 potential treatments strategies of DPN.

375

376 **Conclusion**

377 In this study, we used HFD to induce a mouse model of diabetic peripheral neuropathy. We
378 observed key metabolic dysfunctions indicative of T2D in these animals. Behavioral analysis
379 uncovered early-onset of peripheral neuropathy with mechanical hypoalgesia and thermal
380 hyperalgesia. We also identified L1CAM as a new marker of nociceptive Schwann cells.
381 Interestingly, we observed a significant decrease in number of nociceptive Schwann cells and
382 their extensions in the foot skin of neuropathic mice, highlighting the vulnerability of these
383 cells in T2D conditions. Overall, our analyses recapitulate the early events in diabetic
384 peripheral neuropathy pathophysiology, paving the way for future investigations into the
385 molecular mechanisms underlying nociceptive Schwann cells alterations and potential
386 strategies to thwart this debilitating complication of diabetes.

Acknowledgment

We thank Dr Douglas Wright and Janelle Ryals for their assistance with the PGP9.5 immunohistochemistry. We thank Dr Aziz Moqrich for providing the PLPcreERT2 and Ai14 mice.

Data availability

The authors confirm that the data supporting the findings of this study are available within the article and its supplementary materials. Further information and requests may be sent to the corresponding author.

Funding

This research was supported by a grant funded by Inserm, Paris, France [ATIP-AVENIR].

Contribution statement

All authors meet the ICMJE uniform requirements for authorship and approved the final version of the manuscript. GR and SB conceptualized the study and contributed to study design. GR, AKJ, AP and SB participated in skin biopsy and data acquisition. MPG and KT performed plasma insulin and leptin concentrations measurements. GR and MB participated in OGTT. GR and AKJ participated in data analysis. MB and CP took care of the maintenance of the animals. GL and MPG helped in critical reading of the article. All authors contributed to manuscript drafting, editing and revision. GR and SB wrote the original draft and all authors revised the manuscript. SB accepts full responsibility for the work and/or the conduct of the study, had access to the data, and controlled the decision to publish.

414 **Bibliography**

415 1. Feldman EL, Nave K-A, Jensen TS, Bennett DLH (2017) New Horizons in Diabetic Neuropathy:
416 Mechanisms, Bioenergetics, and Pain. Neuron 93(6):1296–1313.
417 https://doi.org/10.1016/j.neuron.2017.02.005

418 2. Themistocleous AC, Ramirez JD, Shillo PR, et al (2016) The Pain in Neuropathy Study (PiNS): a
419 cross-sectional observational study determining the somatosensory phenotype of painful and
420 painless diabetic neuropathy. Pain 157(5):1132–1145.
421 https://doi.org/10.1097/j.pain.0000000000000491

422 3. Callaghan BC, Cheng HT, Stables CL, Smith AL, Feldman EL (2012) Diabetic neuropathy: clinical
423 manifestations and current treatments. Lancet Neurol 11(6):521–534.
424 https://doi.org/10.1016/S1474-4422(12)70065-0

425 4. Margolis DJ, Malay DS, Hoffstad OJ, et al (2011) Incidence of diabetic foot ulcer and lower
426 extremity amputation among Medicare beneficiaries, 2006 to 2008: Data Points #2. In: Data
427 Points Publication Series. Agency for Healthcare Research and Quality (US), Rockville (MD)

428 5. Green AQ, Krishnan S, Finucane FM, Rayman G (2010) Altered C-fiber function as an indicator of
429 early peripheral neuropathy in individuals with impaired glucose tolerance. Diabetes Care
430 33(1):174–176. https://doi.org/10.2337/dc09-0101

431 6. Malik RA, Tesfaye S, Newrick PG, et al (2005) Sural nerve pathology in diabetic patients with
432 minimal but progressive neuropathy. Diabetologia 48(3):578–585.
433 https://doi.org/10.1007/s00125-004-1663-5

434 7. Lauria G, Faber CG, Cornblath DR (2022) Skin biopsy and small fibre neuropathies: facts and
435 thoughts 30 years later. J Neurol Neurosurg Psychiatry jnnp-2021-327742.
436 https://doi.org/10.1136/jnnp-2021-327742

437 8. Abdo H, Calvo-Enrique L, Lopez JM, et al (2019) Specialized cutaneous Schwann cells initiate
438 pain sensation. Science 365(6454):695–699. https://doi.org/10.1126/science.aax6452

439 9. Hu X, Agarwal N, Zhang M-D, et al (2022) Identification and quantification of nociceptive
440 Schwann cells in mice with and without Streptozotocin-induced diabetes. J Chem Neuroanat
441 123:102118. https://doi.org/10.1016/j.jchemneu.2022.102118

442 10. Ojeda-Alonso J, Calvo-Enrique L, Paricio-Montesinos R, et al (2023) Sensory Schwann cells set
443 perceptual thresholds for touch and selectively regulate mechanical nociception.
444 2022.02.04.477749

445 11. Rinwa P, Calvo-Enrique L, Zhang M-D, Nyengaard JR, Karlsson P, Ernfors P (2021) Demise of
446 nociceptive Schwann cells causes nerve retraction and pain hyperalgesia. Pain 162(6):1816–
447 1827. https://doi.org/10.1097/j.pain.0000000000002169

448 12. Surwit RS, Kuhn CM, Cochrane C, McCubbin JA, Feinglos MN (1988) Diet-induced type II
449 diabetes in C57BL/6J mice. Diabetes 37(9):1163–1167. https://doi.org/10.2337/diab.37.9.1163

450 13. Leone DP, Genoud S, Atanasoski S, et al (2003) Tamoxifen-inducible glia-specific Cre mice for
451 somatic mutagenesis in oligodendrocytes and Schwann cells. Mol Cell Neurosci 22(4):430–440.
452 https://doi.org/10.1016/s1044-7431(03)00029-0

453 14. Obrosova IG, Li F, Abatan OI, et al (2004) Role of poly(ADP-ribose) polymerase activation in
454 diabetic neuropathy. Diabetes 53(3):711–720. https://doi.org/10.2337/diabetes.53.3.711

455 15. Oh SS, Hayes JM, Sims-Robinson C, Sullivan KA, Feldman EL (2010) The effects of anesthesia on
456 measures of nerve conduction velocity in male C57Bl6/J mice. Neurosci Lett 483(2):127–131.
457 https://doi.org/10.1016/j.neulet.2010.07.076

458 16. Schulz A, Walther C, Morrison H, Bauer R (2014) In vivo electrophysiological measurements on
459 mouse sciatic nerves. J Vis Exp JoVE (86):51181. https://doi.org/10.3791/51181

460 17. Bonin RP, Bories C, De Koninck Y (2014) A simplified up-down method (SUDO) for measuring
461 mechanical nociception in rodents using von Frey filaments. Mol Pain 10:26.
462 https://doi.org/10.1186/1744-8069-10-26

463 18. Hargreaves K, Dubner R, Brown F, Flores C, Joris J (1988) A new and sensitive method for
464 measuring thermal nociception in cutaneous hyperalgesia. Pain 32(1):77–88.
465 https://doi.org/10.1016/0304-3959(88)90026-7

466 19. Yeomans DC, Proudfit HK (1996) Nociceptive responses to high and low rates of noxious
467 cutaneous heating are mediated by different nociceptors in the rat: electrophysiological
468 evidence. Pain 68(1):141–150. https://doi.org/10.1016/S0304-3959(96)03177-6

469 20. Deuis JR, Vetter I (2016) The thermal probe test: A novel behavioral assay to quantify thermal
470 paw withdrawal thresholds in mice. Temp Multidiscip Biomed J 3(2):199–207.
471 https://doi.org/10.1080/23328940.2016.1157668

472 21. Bourane S, Grossmann KS, Britz O, et al (2015) Identification of a spinal circuit for light touch
473 and fine motor control. Cell 160(3):503–515. https://doi.org/10.1016/j.cell.2015.01.011

474 22. Gomez-Sanchez JA, Pilch KS, van der Lans M, et al (2017) After Nerve Injury, Lineage Tracing
475 Shows That Myelin and Remak Schwann Cells Elongate Extensively and Branch to Form Repair
476 Schwann Cells, Which Shorten Radically on Remyelination. J Neurosci Off J Soc Neurosci
477 37(37):9086–9099. https://doi.org/10.1523/JNEUROSCI.1453-17.2017

478 23. Biessels GJ, Bril V, Calcutt NA, et al (2014) Phenotyping animal models of diabetic neuropathy: a
479 consensus statement of the diabetic neuropathy study group of the EASD (Neurodiab). J
480 Peripher Nerv Syst JPNS 19(2):77–87. https://doi.org/10.1111/jns5.12072

481 24. Yu Y (2021) Gold Standard for Diagnosis of DPN. Front Endocrinol 12:719356.
482 https://doi.org/10.3389/fendo.2021.719356

483 25. Sumner CJ, Sheth S, Griffin JW, Cornblath DR, Polydefkis M (2003) The spectrum of neuropathy
484 in diabetes and impaired glucose tolerance. Neurology 60(1):108–111.
485 https://doi.org/10.1212/wnl.60.1.108

486 26. Coppey L, Davidson E, Lu B, Gerard C, Yorek M (2011) Vasopeptidase inhibitor ilepatril
487 (AVE7688) prevents obesity- and diabetes-induced neuropathy in C57Bl/6J mice.
488 Neuropharmacology 60(2–3):259–266. https://doi.org/10.1016/j.neuropharm.2010.09.008

489 27. Sajic M, Rumora AE, Kanhai AA, et al (2021) High Dietary Fat Consumption Impairs Axonal
490 Mitochondrial Function In Vivo. J Neurosci 41(19):4321–4334.
491 https://doi.org/10.1523/JNEUROSCI.1852-20.2021

492 28. Vincent AM, Hayes JM, McLean LL, Vivekanandan-Giri A, Pennathur S, Feldman EL (2009)
493 Dyslipidemia-induced neuropathy in mice: the role of oxLDL/LOX-1. Diabetes 58(10):2376–
494 2385. https://doi.org/10.2337/db09-0047

495 29. Ziegler D, Papanas N, Zhivov A, et al (2014) Early detection of nerve fiber loss by corneal
496 confocal microscopy and skin biopsy in recently diagnosed type 2 diabetes. Diabetes
497 63(7):2454–2463. https://doi.org/10.2337/db13-1819

498 30. Arimura A, Deguchi T, Sugimoto K, et al (2013) Intraepidermal nerve fiber density and nerve
499 conduction study parameters correlate with clinical staging of diabetic polyneuropathy.
500 Diabetes Res Clin Pract 99(1):24–29. https://doi.org/10.1016/j.diabres.2012.09.026

501 31. Nolano M, Tozza S, Caporaso G, Provitera V (2020) Contribution of Skin Biopsy in Peripheral
502 Neuropathies. Brain Sci 10(12):989. https://doi.org/10.3390/brainsci10120989

503 32. Shun C-T, Chang Y-C, Wu H-P, et al (2004) Skin denervation in type 2 diabetes: correlations with
504 diabetic duration and functional impairments. Brain J Neurol 127(Pt 7):1593–1605.
505 https://doi.org/10.1093/brain/awh180

506 33. Smith AG, Ramachandran P, Tripp S, Singleton JR (2001) Epidermal nerve innervation in
507 impaired glucose tolerance and diabetes-associated neuropathy. Neurology 57(9):1701–1704.
508 https://doi.org/10.1212/wnl.57.9.1701

509 34. De Logu F, Nassini R, Materazzi S, et al (2017) Schwann cell TRPA1 mediates neuroinflammation
510 that sustains macrophage-dependent neuropathic pain in mice. Nat Commun 8(1):1887.
511 https://doi.org/10.1038/s41467-017-01739-2

512 35. Raut NGR, Maile LA, Oswalt LM, et al (2024) Schwann cells modulate nociception in
513 neurofibromatosis 1. JCI Insight 9(2). https://doi.org/10.1172/jci.insight.171275

514 36. Reinisch CM, Traxler H, Piringer S, Tangl S, Nader A, Tschachler E (2008) Rarefaction of the
515 Peripheral Nerve Network in Diabetic Patients Is Associated With a Pronounced Reduction of
516 Terminal Schwann Cells. Diabetes Care 31(6):1219–1221. https://doi.org/10.2337/dc07-1832

517 37. Liu Y-P, Shao S-J, Guo H-D (2020) Schwann cells apoptosis is induced by high glucose in diabetic
518 peripheral neuropathy. Life Sci 248:117459. https://doi.org/10.1016/j.lfs.2020.117459

519 38. Wang X, Xu G, Liu H, et al (2023) Inhibiting apoptosis of Schwann cell under the high-glucose
520 condition: A promising approach to treat diabetic peripheral neuropathy using Chinese herbal
521 medicine. Biomed Pharmacother 157:114059. https://doi.org/10.1016/j.biopha.2022.114059

522 39. Callaghan BC, Little AA, Feldman EL, Hughes RAC (2012) Enhanced glucose control for
523 preventing and treating diabetic neuropathy. Cochrane Database Syst Rev 6(6):CD007543.
524 https://doi.org/10.1002/14651858.CD007543.pub2

525 40. Jende JME, Groener JB, Rother C, et al (2019) Association of Serum Cholesterol Levels With
526 Peripheral Nerve Damage in Patients With Type 2 Diabetes. JAMA Netw Open 2(5):e194798.
527 https://doi.org/10.1001/jamanetworkopen.2019.4798

528 41. Rumora AE, Kim B, Feldman EL (2022) A Role for Fatty Acids in Peripheral Neuropathy
529 Associated with Type 2 Diabetes and Prediabetes. Antioxid Redox Signal 37(7–9):560–577.
530 https://doi.org/10.1089/ars.2021.0155

42. Stino AM, Rumora AE, Kim B, Feldman EL (2020) Evolving concepts on the role of dyslipidemia, bioenergetics, and inflammation in the pathogenesis and treatment of diabetic peripheral neuropathy. J Peripher Nerv Syst JPNS 25(2):76–84. https://doi.org/10.1111/jns.12387

537 **Figure Legends**

538

539 **Figure 1: Study design and HFD-induced dyslipidemia.** (**A**) Study Design used to assess the
540 effect of a HFD (45% kcal %fat) vs. a control diet (10% kcal %fat) in two groups of mice
541 (n=10/group). (**B**) Body weight of control diet-fed mice and HFD-fed mice during the 16 weeks
542 of diet. (**C**) Leptinemia of control and HFD mice at 16 weeks of diet. (**D**) Plasma levels
543 triglycerides of control and HFD mice at 16 weeks of diet. (**E**) Total cholesterolemia of control
544 and HFD mice at 16 weeks of diet. *P < 0.05, **P < 0.01, ***P < 0.001: control diet vs. HFD.
545 Data are presented as means ± SEM.

546

547 **Figure 2: HFD-induced impaired glucose tolerance. (A)** Fasting blood glucose of control diet-
548 fed mice and HFD-fed mice at 16 weeks of diet. **(B)** Percentage of glycated hemoglobin
549 (HbA1c) of control diet-fed mice and HFD-fed mice at 16 weeks of diet. **(C)** Plasma insulin of
550 control diet-fed mice and HFD-fed mice at 16 weeks of diet. **(D)** Oral glucose tolerance test
551 (OGTT) curves performed at 16 weeks of diet in control and HFD-fed mice. **(E)** Area under the
552 curve (AUC) during OGTT for control diet-fed mice and HFD-fed mice. *P < 0.05, **P < 0.01,
553 ***P < 0.001: control diet vs. HFD. Data are presented as means ± SEM (n=10/group).

554

555 **Figure 3: Nerve conduction studies. (A)** Motor nerve conduction velocity (MNCV) performed
556 at 16 weeks of diet in control and HFD-fed mice. **(B)** Sensory nerve conduction velocity (SNCV)
557 performed at 16 weeks of diet in control and HFD-fed mice**.** Data are presented as means ±
558 SEM (n=10/group).

559

560 **Figure 4: Mechanical and thermal sensitivity changes induced by HFD. (A)** Quantification of
561 static mechanical sensitivity was assessed every 4 weeks in control and HFD-fed mice using
562 von Frey filaments. **(B)** Quantification of thermal sensitivity by Hargreaves test every 4 weeks
563 in control and HFD-fed mice. **(C)** Quantification of haptic mechanical sensitivity by brush test
564 every 4 weeks in control and HFD-fed mice. **(D)** Quantification of acute mechanical pain by
565 pinprick test every 4 weeks in control- and HFD-fed mice. **P < 0.01, ***P < 0.001: control
566 diet vs. HFD. #P < 0.05, ##P < 0.01: HFD 4weeks vs. HFD 8, 12 or 16 weeks. Data are presented
567 as means ±SEM (n=10/group).

568

569 **Figure 5: HFD-induced small nerve fiber and nociceptive Schwann cells degeneration in the**
570 **foot skin.** (**A**) PGP9.5 immunofluorescence with DAPI staining in foot skin section of control
571 (n=5) and HFD-fed mice (n=5). Arrowhead indicate nerve fibers in the epidermis of the foot
572 skin. (**B**) Quantification of IENFD is presented as the number of fibers/mm of epidermis. (**C**)

573 L1CAM immunofluorescence colocalized with Sox10 andS100β classical markers of
574 nociceptive Schwann cells in the foot skin. (**D**) L1CAM immunofluorescence colocalized with
575 Td-tomato expressing nociceptive Schwann cells in a tamoxifen-induced PLP-
576 CreERT2;R26TdTomato double transgenic mouse. Arrowhead indicate nociceptive Schwann
577 cells and their cellular extensions at the border of the epidermis and dermis. (**E**) L1CAM
578 immunofluorescence with DAPI staining in foot skin section of control (n=5) and HFD-fed mice
579 (n=5). Arrows indicate nociceptive Schwann cells and their cellular extensions at the border of
580 the epidermis and the dermis. **(F**) Mean fluorescence intensity quantification of L1CAM
581 immunostaining at the localization of nociceptive Schwann cells (at the border of epidermis
582 and dermis). (**G**) Quantification of L1CAM-positive cells and their cellular extensions presented
583 in number/mm of epidermis. $^{**}P < 0.01$, $^{***}P < 0.001$: control diet vs. HFD. Data are
584 presented as means ± SEM. Scale bar: 50 µm.

585

586